Methodology to Generate a Reluctance Network Applied to Permanent Magnet Synchronous Generators

João Vitor Gerevini Kasper[1] (ID), Patrick Kuo-Peng[1] (ID), Thiago de Paula Machado Bazzo[2] (ID), Gustavo Garbelini de Menezes[2] (ID)

[1]GRUCAD/EEL/CTC, Federal University of Santa Catarina, Florianópolis, SC, Brazil
joaovitorgk_21@hotmail.com, patrick.kuo.peng@ufsc.br
[2]PPGSE – Federal University of Technology - Paraná (UTFPR), Curitiba, PR, Brazil

Abstract— **This paper presents a methodology for the generation of a static reluctance network, with magnetomotive sources only in the rotor, applied in the analysis and design of surface mounted permanent magnet synchronous generators. In the analysis stage, this network can provide the magnetic flux in several points of the generator, enabling an estimate of the generator performance. In the design process, on the other hand, it provides the armature linkage flux and hence the induced EMF can be calculated. It is worth mentioning that the proposed methodology makes use of a good discretization level (high number of elements) on the teeth tips and in the air gap of the generator, in order to get better precision on the flux modeling of these regions. The main contribution of this paper is to present the development process of a static reluctance network applied to surface mounted permanent magnets synchronous generators with different dimensions. The proposed model has proved to be robust and flexible as it can be seen in the results. The reluctance network (RN) developed with the proposed methodology presented in this paper shows low variations of the magnetic flux values, when compared with finite element simulations.**

Index Terms— **Permanent Magnet Synchronous Generators; Reluctance Network; Finite Elements Method; Electric Machine Modeling.**

I. INTRODUCTION

Permanent Magnet Synchronous Generators (PMSG) are machines applied in various fields of electromechanical energy conversion. By using Permanent Magnets (PM) on the rotor to produce the machine flux, this type of generator has some advantages when compared to wound-rotor synchronous generators: higher efficiency (no losses on rotor windings) and higher torque density (smaller volume and less active material mass). Nonetheless, PMSG does not allow the adjustment of the induced voltage when the load varies and has a higher cost when compared to its equivalent wound-rotor [1], [2]. Magnetic flux analysis can be performed using reluctance networks, providing more accurate results than analytical models (faster method), with a lower computational cost than the Finite Element Method (FEM) (more accurate method) [1], [3]. In a single isolated simulation, this might not seem like a big advantage. However, in an optimization process, where the solution of the

problem must be found multiple times, the total solution time gains more relevance as it takes much longer to be completed.

Reluctance networks (RN) can be static or multi-static. Static RNs calculate the magnetic flux for a single rotor position and do not account for rotor movement. There are static RN's that model only the rotor magnetomotive sources, which are placed in position where the flux linked by the armature windings is maximum and the flux waveform is considered perfectly sinusoidal. Therefore, the flux obtained represents the peak value of the waveform [4]. Once the linked flux is obtained from the RN, the no-load induced voltage can be calculated (neglecting the harmonic content) considering the frequency and the number of turns of the armature. To obtain the terminal voltage, the voltage drop due to the armature reaction has to be subtracted, which can be done using algebraic equations, once the direct axis (X_d) and quadrature axis (X_q) reactances are known.

These reactances can be obtained by analytic methods (when the machine geometry is simple), with FEM, or even using two static RN with magnetomotive sources only in the stator (one with the rotor aligned to direct axis and other with the rotor aligned to quadrature axis) [5]. The net flux value can be also obtained by two static RN having both rotor and stator magnetomotive sources and, therefore, the reactance calculation is not needed to determine the terminal voltage value [6]. In addition, for the design of synchronous generators, static reluctance networks can include the calculation of hysteresis [7] and eddy current losses [8]. However, as they are static models that neglect harmonics, large errors are expected in the loss calculations.

Multi-static reluctance networks, on the other hand, are adaptative models that take into account the rotor movement. In these networks, air-gap reluctances adapt as the rotor position changes, in this way, for each new rotor position the corresponding RN needs to be solved. By providing the magnetic flux for different rotor positions, this type of modeling allows the estimation of the linked flux waveform in electric machines [9], unlike the static model, where only its magnitude can be obtained. In a multi-static model with sources in the rotor it is possible to obtain the waveform of the no-load voltage induced in the armature coils. With this approach, the use of an extra model (analytic method, RN or FEM) is necessary to find the direct axis (X_d) and (X_q) quadrature axis reactances [10]-[12] for the computation of the machine terminal voltage. In a complete multi-static model, that is with rotor and stator magnetomotive sources, it is possible to find the net flux linked by the armature windings in different rotor positions. Thus, the terminal voltage waveform can be obtained under load operation [13]-[17]. It is worth mentioning that this approach also allows the calculation of iron losses considering all the harmonics content present in the generator, therefore, the calculations of the losses is more accurate.

Most works that propose RN's do not present clearly the development of the model used. Furthermore, most of the reluctance networks are presented as tools for analysis or design of electrical machines. The RN's found in the literature can be used to calculate the magnetic flux and density, to

determine the induced and the terminal voltage of the machine, to estimate the hysteresis and eddy losses and to determine the torque produced by any electromagnetic devices [4]-[17]. Due to its great relevance in analysis and design of electric machines, the main objective of this paper is to present, in detail, the generating process of a static RN, more precisely, a network with magnetomotive sources only in the rotor. The calculations of length and area of each reluctance of the network and the mathematical model developed to make the network parametric are the main contributions of this paper. The network developed with the proposed methodology is applied to a surface-mounted permanent magnet synchronous generator (SMPMSG) but can be applied to other types of permanent magnet generators (with embedded magnet, external rotor, etc.).

II. CHARACTERISTICS OF THE SMPMSG

A. *Main dimension quantities needed for the RN generation*

The proposed methodology to generate a RN is applied to a surface mounted permanent magnets synchronous generator (SMPMSG). The rotor of a permanent magnet synchronous generator is made of a magnetic core, either a single piece or composed of magnetic steel plates. The permanent magnets are arranged and fixed to this structure and are responsible to create the main magnetic flux of the generator. The constructive characteristics of the stator of a PMSG are similar to those of a wound-rotor generator and even to those of an induction motor. The ferromagnetic core of the stator is formed by stacked sheets to reduce iron losses [2]. These magnetic steel sheets have slots where the armature windings, usually copper, are allocated. Fig. 1 shows the main dimensions of an SMPMSG, which are used in RN modeling.
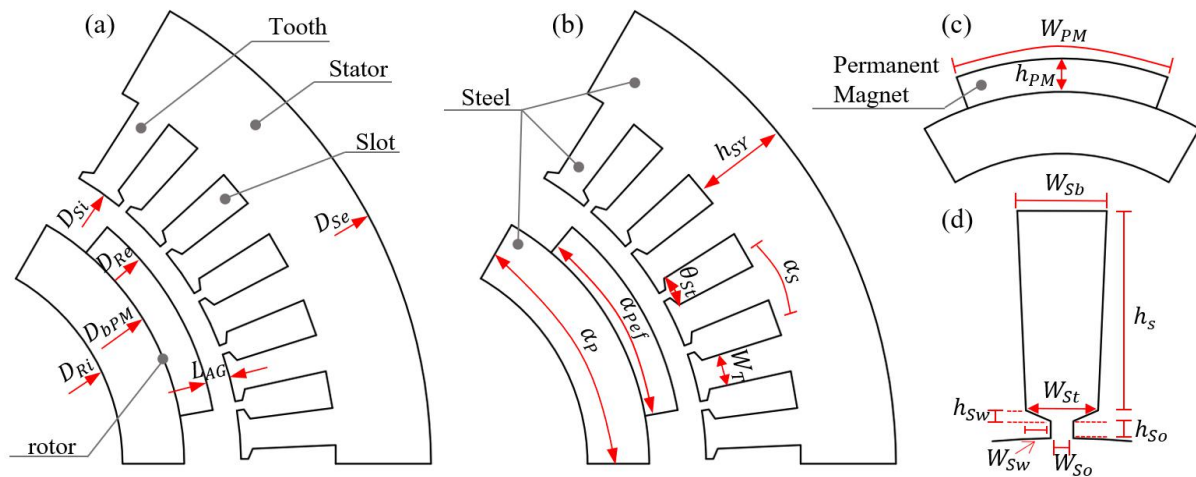

Fig. 1. Main Dimensions of the SMPMSG.

Fig. 1(a) shows the dimension of the following quantities: rotor internal diameter (D_{Ri}), the diameter at the base of the permanent magnet (D_{bPM}), rotor external diameter (D_{Re}), stator internal diameter (D_{Si}) and stator external diameter (D_{Se}). Another important parameter is the air gap length (L_{AG}) of the generator, which is the radial distance between a pole and the stator teeth.

Fig. 1(b) shows the pole pitch (α_P), the effective pole pitch (α_{Pef}), the slot pitch (α_S) and the angle occupied by the top of one slot (θ_{St}), the tooth width (W_T) and the stator yoke height (h_{SY}). Fig. 1(c) and (d) present, in detail, dimensions of the permanent magnet and stator slots, respectively. In Fig. 1(c) can be seen the PM height (h_{PM}) and the width of the PM arc (W_{PM}). In Fig. 1(d) are the height of the slot opening (h_{So}), the height of the slot wedge (h_{Sw}), the height of the slot (h_s) and the width of the slot opening (W_{So}), all of which determine the shape of the stator teeth and are used to calculate the reluctances of slot openings and tooth tips, while the slot wedge width (W_{Sw}) is very important when modeling the stator flux. The width on the bottom (W_{Sb}) and on the top (W_{St}) of the slot are used to calculate the stator yoke and tooth tips reluctances of the machine.

B. Permanent Magnets modelling for SMPMSG

Permanent magnets are materials capable of storing 'an important value of' a residual magnetic field after undergoing the magnetization process. Two important points of the hysteresis loop of a permanent magnet can be highlighted: the remanent induction (B_r) – or remanent flux density – and the coercive force (H_c). The remanent induction defines the amount of flux density that the material retains when the external field (which magnetized it) is removed; while the coercive force defines the magnitude of magnetic field that must be applied to it for its demagnetization. These two points, presented in Fig. 2, define the demagnetization curve of permanent magnets. The flux density produced by the magnet depends on the magnetic circuit of which it is a part of. Therefore, the operative induction of the magnet is not equal to the remanent induction.

Still in Fig. 2, three operating points can be highlighted in the second quadrant of the hysteresis loop (or B-H loop), each one with projections on the flux density and magnetic field axes. Each of them has two coordinates H_{op} and B_{op} which are known as the operative field and induction of the magnets, that is, the ordered pair (H_5, B_5) provides the operative values of magnetic induction and magnetic field, considering the permeance coefficient equal to the P_{c5}, for example. All points are determined by the intersection between the load line and the demagnetization curve. Varying the load line slope, results in different field and operative induction values (H_{op}, B_{op}) and, therefore, a different operating point. The slope's magnitude of these lines is known as the permeance coefficient (P_c) [1].

$$P_c = \frac{B_5}{\mu_0 \bullet |H_5|} = \frac{h_{PM} \bullet A_g}{f_{LKG} \bullet L_{AG} \bullet A_m} \tag{1}$$

where μ_0 is the permeability of vacuum, h_{PM} is the PM height, $f_{LKG} = \phi_{AG}/\phi_{PM}$ is the coefficient of leakage flux (being ϕ_{AG} and ϕ_{PM} the flux crossing the air gap and the permanent magnet, respectively), L_{AG} is the length of the air gap, A_g the area crossed by the flux in air gap and A_m the area crossed by the flux in permanent magnet. The demonstration of (1) can be found in chapter 4 of [1].

Considering that: the permeability of iron is infinitely greater than that of air, there are no flux leakage in the air gap and all flux produced by de permanent magnets crosses the air gap, it is possible to simplify this equation.

$$P_c = \frac{h_{PM}}{L_{AG}} \qquad (2)$$

All points of the permanent magnet curve can be found by varying the value of the permeance coefficient; thereby, the operative induction provided by the magnet can be calculated as a function of the permeance coefficient. In order to obtain an expression to calculate the operating point of the magnet as a function of the permeance coefficient, as shown in (2).
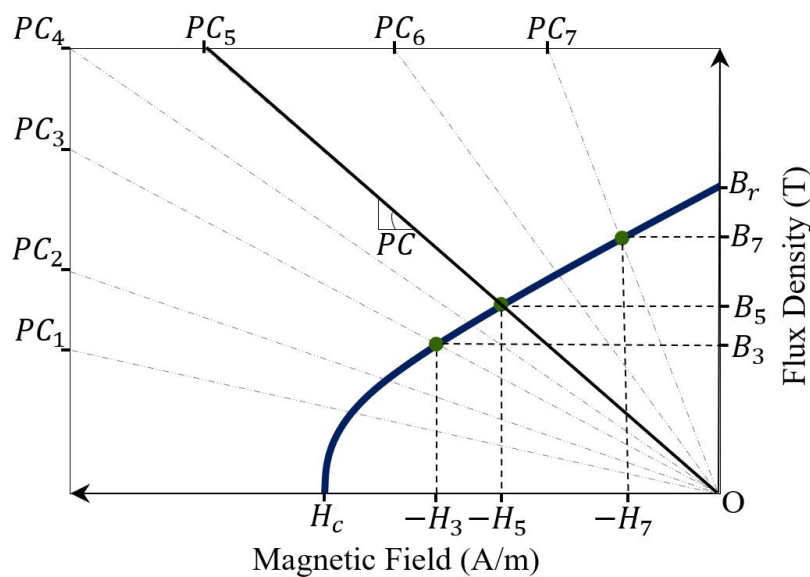

Fig. 2. Second quadrant of the PM B-H loop.

III. RELUCTANCE NETWORK GENERATION

Reluctance networks are magnetic circuits with passive and active elements, used to model the magnetic flux paths in electromagnetic devices. These elements depend mainly on some characteristics such as: magnetic induction, machine geometry, number of turns, material properties and magnetic flux intensity. The active elements of the network are responsible for modeling the magnetomotive sources which are for example in PMSG, the stator coils and the rotor magnets. On the other hand, the passive elements are used to model the flux paths in the ferromagnetic parts of the machines and the flux in the air. The calculation of the reluctances depends on the dimensions of the machine and the characteristics of the B-H curve of the material resulting to a non-linear problem [3], since the values of the iron reluctances vary depending on the value of the flux density.

Given an already defined RN, with the number of elements and meshes adjusted as desired, the objective is to calculate the magnetic flux that flows through all the elements present in the RN. To compute the value of the fluxes in all the reluctances present in the network, it is necessary to solve a system of (2). This system of equations is obtained by applying mesh analysis to the RN [18].

$$[\varphi] = [R]^{-1} \bullet [F_{mm}] \tag{3}$$

in which $[\varphi]$ is the vector of magnetic fluxes flowing in the branches of the reluctance network, $[R]^{-1}$ is the inverse of the reluctance matrix and $[F_{mm}]$ the vector of the magnetomotive sources in the network. Each reluctance in the iron or in the air gap of the RN represents an area (A_R) and a length (l_r), that are calculated according to the equation below:

$$R = \frac{l_r}{\mu_0 \bullet \mu_r \bullet A_R} \tag{4}$$

where μ_r is the relative magnetic permeability of the material, at a given flux density value, and μ_0 is the magnetic permeability of the air. The magnetomotive sources present in the network are related only to the permanent magnets, thus, their values are defined by taking into account the operative induction of the magnet (B_{op}), the magnetic permeability of the material, the magnetic permeability of the air and the length that this source models (l_s), i.e., the length of the magnet.

$$F_{mm} = \frac{B_{op}}{\mu_0 \bullet \mu_r} \bullet l_s \tag{5}$$

The objective of this reluctance network is to model the significant flux paths of one of the magnetic flux loops present in a PMSG operating at no load. A simulation with the FEM, using the EFCAD software [19] for example, is carried out in order to analyze these significant flux paths. The FEM is used to develop the reluctance network, where a single simulation of the machine is made. Once is completely developed, the reluctance network can be applied to other similar machines, without any additional effort.
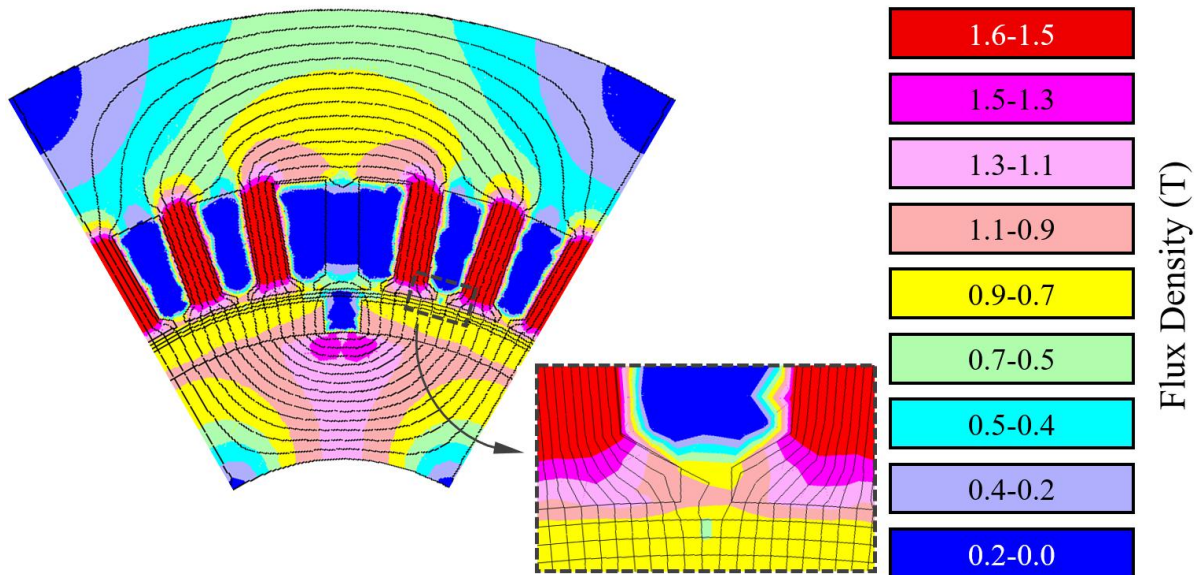

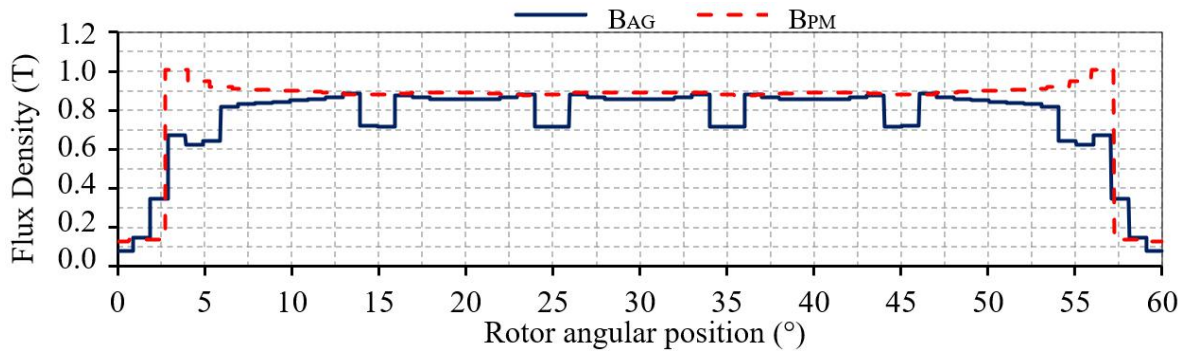Fig. 3. Magnetic flux density distribution on the PMSG at no load.

Fig. 4. Magnetic flux density curves on the air gap and on the center of permanent magnet.

Through the analysis of the magnetic flux paths present in the PMSG, seen in Fig. 3, it is possible to define the RN topology and select which regions of the generator need a greater degree of refinement (use of a greater number of reluctances). As excepted, the radial flux component of the central tooth (between the two magnets of different polarity) is much smaller in relation to the other teeth of the machine. Hence, the modeling of the radial flux present in this tooth is not considered. On the other hand, the transverse flux through the tip of the central tooth has significant value and must be included in the modeling.

The air gap is an important region of the generator. It is where the magnetic flux supplied by the magnets crosses and reaches the stator of the machine. Note that, below of the slot opening in the air gap (B_{AG}), the magnetic flux behaves more irregularly, when compared to the flux in the center of permanent magnets (B_{PM}), as seen in Fig. 4. Consequently, the air gap region and the slot openings receive a greater degree of refinement than the regions of iron and magnets, mentioned above. Finally, it should be noted that there are no significant magnetic flux lines in the PMSG slots. Hence, the stray flux in the slots is not modeled.

A. Proposed Mathematical Model for the Reluctances of the Network

The number and orientation (radial or transversal) of each reluctance was based on the analysis of the behavior of the magnetic flux in different regions of the generator (Fig. 3). The magnetic flux was observed in the following regions of the PMSG: in the rotor yoke, in the permanent magnets, in the air gap below the stator teeth, in the slot openings, at the tip of the stator teeth, in the body of the stator teeth and in the stator yoke. According to the behavior of the magnetic flux in these regions, the number and orientation of reluctances for each of these regions was chosen.

The proposed RN has 316 elements, being 268 reluctances and 48 magnetomotive sources. Of this total reluctances, most (139) are used to model the air gap, the slot openings and the leakage fluxes between the magnets, while the remaining (129) models the other regions of the generator that are composed of iron: stator, rotor and machine teeth. Fig. 5 presents the proposed reluctance network, to model the magnetic flux of one of the flux loops present in a PMSG operating at no load. It is also possible to observe how the different parts of the generator are numbered: magnets, teeth and slot openings, from left to right. The teeth numeration starts with tooth 1 (T_1) and ends with tooth 7 (T_7),

as well as the numbering of slot openings, which starts at slot opening 1 (W_{so1}) and ends at slot opening 6 (W_{so6}). Finally, the halves of the magnets in the rotor are numbered as magnet 1 (P_{M1}) and magnet 2 (P_{M2}).
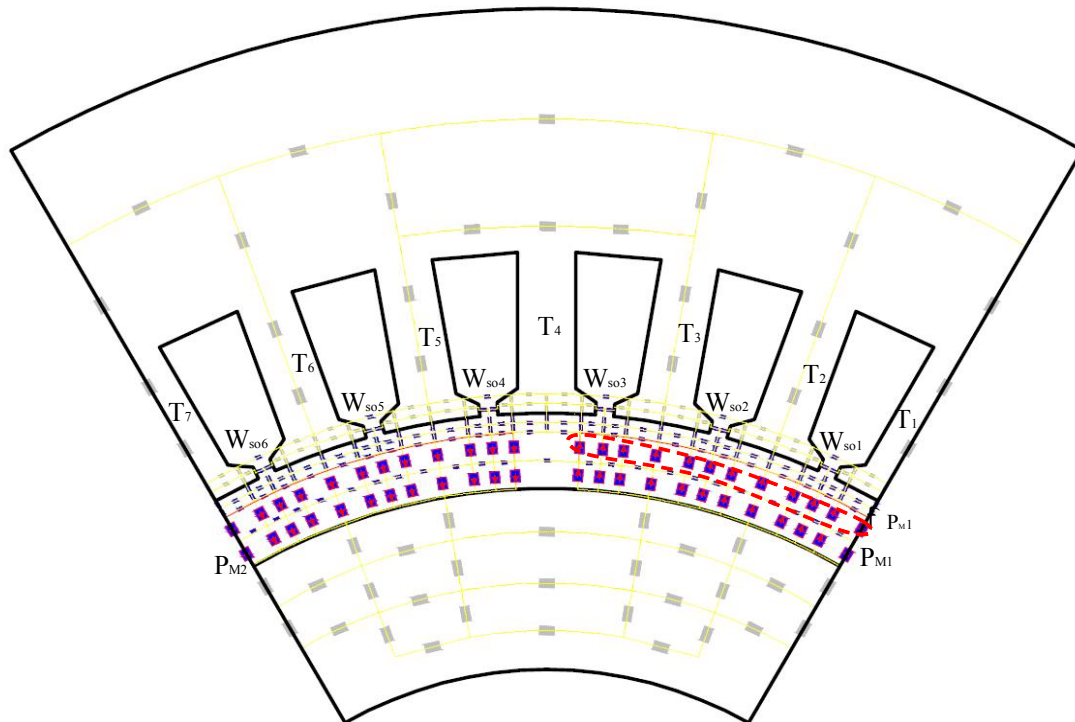

Fig. 5. Reluctance network proposed for modeling of the PMSG.

Fig. 6 brings, in detail, the reluctances used to model: the stator yoke (S_y), the tooth body (T_b), the rotor yoke (R_y), the tooth tips (T_t), the air gap below the teeth (A_g) and the slot openings (S_o), respectively. Fig. 6(a) shows the reluctances used to represent the magnetic flux along half of the stator yoke and in the body of half of a tooth. Three reluctances are used to model the radial flux paths of each tooth of the machine: two in the body of each tooth (T_b) and one in the "root" of the tooth (T_R). The flux paths in the stator yoke are modeled with eight reluctances. In this region, the characteristic direction of most of the magnetic flux is transversal.

In Fig. 6(b), it can be seen that thirteen reluctances are employed to model the part of the rotor yoke below magnet 1 and three reluctances are used to model the center of the rotor yoke. Analyzing the flux in the yoke, below the magnet, the reluctances should be radially arranged, while in the center of the rotor yoke, they should be arranged transversely. The use of this grid allows the representation of magnetic flux components in two directions.
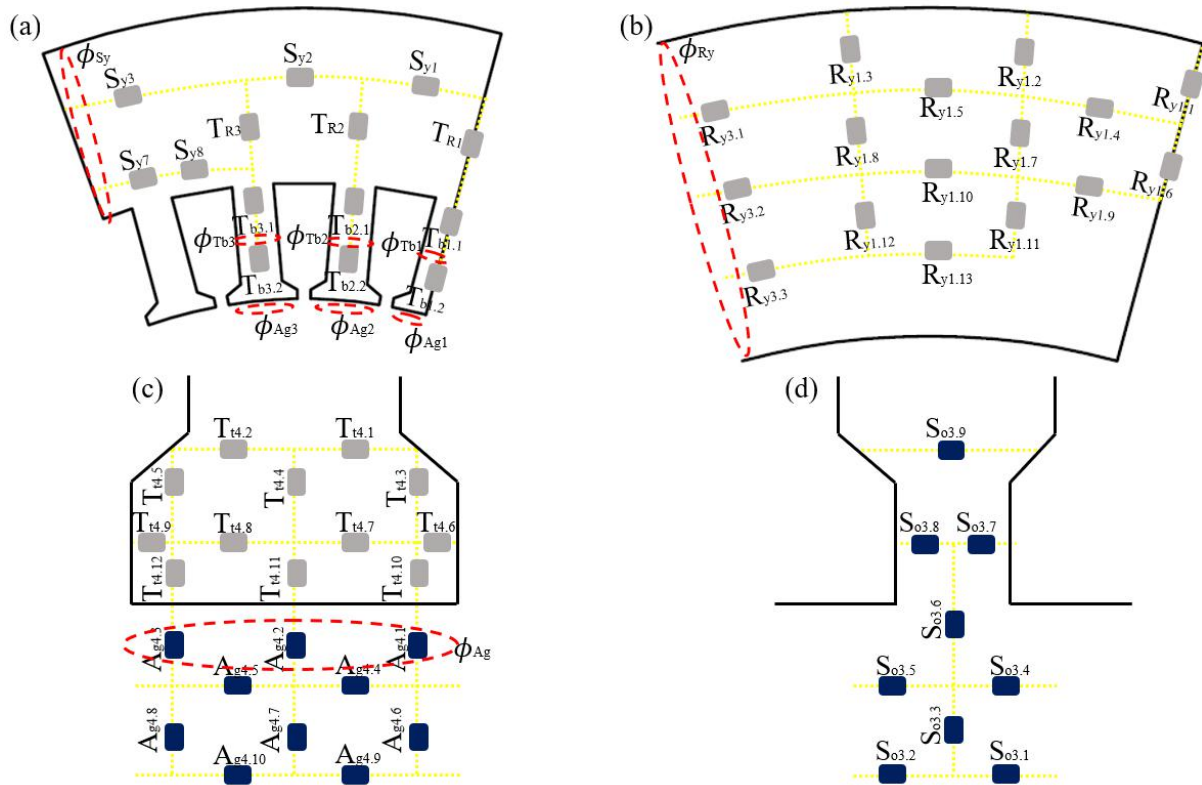
Fig. 6. Refinement degree in different regions of the reluctance network.

Fig. 6 (c) presents the reluctances used to model the air gap below each tooth and the tooth tip. For the air gap region below each tooth, 10 reluctances are used, while at the tip, 12 reluctances are used. In both cases, there are radial and transverse magnetic flux paths, a characteristic also observed in the detail of this region, seen in the flux density map (Fig. 3). Finally, Fig. 6 (d) shows the reluctances applied in the modeling of the slot openings, which are nine in total. In this case, there is a greater number of reluctances modeling the transverse flow than the radial flow. This choice is also based on the careful analysis of the machine flux density map.

Each reluctance, seen in Fig. 5 or in detail in Fig. 6, is represented by a length and an area. Table I presents the expressions used to calculate the lengths and areas of iron reluctances. It is worth noting that the expressions used for the reluctances of the tip of tooth 4 can be used to calculate the reluctances of the tips of teeth: 2, 3, 5 and 6. In the case of teeth 1 and 7, the reluctances aligned with the center of the tooth have the areas divided by two, as they model only half of a tooth. In addition, only 7 reluctances are used on each tooth tip: 3 transverse flow and 4 radial flow reluctances. Other equivalent expressions that can be applied to the undisclosed reluctances of the network are presented at the bottom of Table I.

TABLE I. LENGTH AND AREA OF IRON RELUCTANCES

Reluctance	Length (m)	Area (m²)
$T_{t1.1}\ T_{t1.2}$	$\dfrac{h_S}{2}$	$\dfrac{W_T}{2} \bullet L_A$
$T_{t2.1}\ T_{t2.2}\ T_{t3.1}\ T_{t3.2}$	$\dfrac{h_S}{2}$	$W_T \bullet L_A$
T_{R1}	$\dfrac{h_{Sy}}{2}$	$\left(\dfrac{W_T}{2} + \dfrac{W_{Sb}}{2}\right) \bullet L_A$
$T_{R2}\ T_{R3}$	$\dfrac{h_{Sy}}{2}$	$\left(\dfrac{W_T}{2} + \dfrac{W_{Sb}}{2}\right) \bullet L_A$
$S_{y1}\ S_{y2}$	$\left(\dfrac{D_{St}}{2} + h_S + \dfrac{h_{Sy}}{2}\right) \bullet \alpha_S$	$h_{Sy} \bullet L_A$
S_{y3}	$\left(\dfrac{D_{St}}{2} + h_S + \dfrac{h_{Sy}}{2}\right) \bullet 2 \bullet \alpha_S$	$3 \bullet \dfrac{h_{Sy}}{4} \bullet L_A$
S_{y8}	$\left(\dfrac{D_{St}}{2} + h_S + \dfrac{h_{Sy}}{2}\right) \bullet \left(\alpha_r - \dfrac{\theta_d}{2}\right)$	$\dfrac{h_{Sy}}{4} \bullet L_A$
S_{y7}	W_T	$\left(h_{Sy} + \dfrac{h_S}{4}\right) \bullet L_A$
$T_{t4.1}\ T_{t4.2}$	$\dfrac{W_T}{2} + \dfrac{W_{Sw}}{2}$	$(h_{Sw}) \bullet L_A$
$T_{t4.3}\ T_{t4.5}$	h_{Sw}	$h_{Sw} \bullet L_A$
$T_{t4.4}$	h_{Sw}	$W_T \bullet L_A$
$T_{t4.6}\ T_{t4.9}$	$\dfrac{W_{Sw}}{2}$	$\left(h_{So} + \dfrac{h_{Sw}}{2}\right) \bullet L_A$
$T_{t4.7}\ T_{t4.8}$	$\dfrac{W_T}{2} + \dfrac{W_{Sw}}{2}$	$h_{So} \bullet L_A$
$T_{t4.10}\ T_{t4.12}$	h_{So}	$W_{Sw} \bullet L_A$
$T_{t4.11}$	h_{So}	$L_d \bullet L_A$
$R_{y1.1}\ R_{y1.2}\ R_{y1.3}\ R_{y1.6}\ R_{y1.7}\ R_{y1.8}$	$\dfrac{H_{cr}}{4}$	$\dfrac{W_{PM}}{6} \bullet L_A$
$R_{y1.4}\ R_{y1.5}\ R_{y1.9}\ R_{y1.10}$	$\left(\dfrac{D_{bPM}}{2} - \dfrac{h_{Sw}}{2}\right) \bullet \dfrac{\alpha_{Pef}}{4}$	$\dfrac{h_{Sw}}{4} \bullet L_A$
$R_{y1.11}$	$\dfrac{h_{Sw}}{2}$	$\dfrac{W_{PM}}{3} \bullet L_A$
$R_{y1.12}$	$\dfrac{h_{Sw}}{2}$	$\dfrac{W_{PM}}{6} \bullet L_A$
$R_{y1.13}$	$\left(\dfrac{D_{bPM}}{2} - \dfrac{h_{Sw}}{2}\right) \bullet \dfrac{\alpha_{Pef}}{4}$	$\dfrac{h_{Sw}}{2} \bullet L_A$

$T_{t7.1}$ and $T_{t7.2}$ equal to $T_{t1.1}$; $T_{t5.1}$, $T_{t5.2}$, $T_{t6.1}$ and $T_{t6.2}$ equal to $T_{t2.1}$; T_{R5} and T_{R6} equal to T_{R2}; T_{R7} equal to T_{R1}; S_{y4} and S_{y5} equal to S_{y1}; S_{y6} equal to S_{y8}; $R_{y2.1}$, $R_{y2.2}$, $R_{y2.3}$, $R_{y2.6}$, $R_{y2.7}$ and $R_{y2.8}$ equal to $R_{y1.1}$; $R_{y2.4}$, $R_{y2.5}$, $R_{y2.9}$ and $R_{y2.10}$ equal to $R_{y1.4}$; $R_{y2.11}$ equal to $R_{y1.11}$; $R_{y2.12}$ equal to $R_{y1.12}$; $R_{y2.13}$ equal to $R_{y1.13}$.

Table II presents the equation for calculating the areas and lengths for the reluctances present in the air gap, slot openings and flux leakage near the magnets (Fig. 5). The same expressions given for the reluctances in slot opening 3 can be applied to all machine slot openings. The expressions used in the air gap below teeth 4 can also be used for the air gap below teeth: 2, 3, 5 and 6. For the air gap below teeth 1 and 7, only 6 reluctances are used, 4 for radial flow and two for axial flow. Regarding the expressions of reluctances $A_{g4.2}$ and $A_{g4.7}$, the only change that must be made is to divide the

reluctance area by two, since, again, only half of the tooth is being modeled. The other equivalent expressions for the leakage reluctances of the magnets are presented at the bottom of Table II.

TABLE II. LENGTH AND AREA OF AIR-GAP RELUCTANCES

Reluctance	Length (m)	Area (m²)
$A_{g4.1}\ A_{g4.3}\ A_{g4.6}\ A_{g4.8}$	$\dfrac{L_{AG}}{2}$	$W_{Sw} \bullet L_A$
$A_{g4.2}\ A_{g4.7}$	$\dfrac{L_{AG}}{2}$	$W_T \bullet L_A$
$A_{g4.4}\ A_{g4.5}\ A_{g4.9}$ $A_{g4.10}$	$\dfrac{W_T}{2}+\dfrac{W_{Sw}}{2}$	$\dfrac{L_{AG}}{2} \bullet L_A$
$S_{o3.1}\ S_{o3.2}\ S_{o3.4}\ S_{o3.5}$	$\dfrac{W_{Sw}}{2}+\dfrac{W_{So}}{2}$	$\dfrac{L_{AG}}{2} \bullet L_A$
$S_{o3.3}$	$\dfrac{L_{AG}}{2}$	$W_{So} \bullet L_A$
$S_{o3.6}$	$\dfrac{L_{AG}}{2}+\dfrac{h_{So}}{2}$	$h_{So} \bullet L_A$
$S_{o3.7}\ S_{o3.8}$	$\dfrac{W_{So}}{2}$	$h_{So} \bullet L_A$
$S_{o3.9}$	$W_{So} + W_{Sw}$	$h_{Sw} \bullet L_A$
$P_{M1.1}\ P_{M1.4}\ P_{M1.5}$ $P_{M1.8}\ P_{M1.9}$	$\left(\dfrac{D_{re}}{2}-\dfrac{h_{PM}}{2}\right) \bullet \left(\dfrac{\theta_T}{2}+\dfrac{\theta_{W_{Sw}}}{2}\right)$	$h_{PM} \bullet L_A$
$P_{M1.2}\ P_{M1.3}\ P_{M1.6}$ $P_{M1.7}\ P_{M1.10}\ P_{M1.11}$	$\left(\dfrac{D_{re}}{2}-\dfrac{h_{PM}}{2}\right) \bullet \left(\dfrac{\theta_{W_{So}}}{2}+\dfrac{\theta_{W_{Sw}}}{2}\right)$	$h_{PM} \bullet L_A$
A_{gD1}	$\left(\dfrac{D_{re}}{2}-\dfrac{h_{PM}}{2}\right) \bullet (\alpha_P - \alpha_{Pef})$	$h_{PM} \bullet L_A$

$P_{M2.1}, P_{M2.4}, P_{M2.5}, P_{M2.8}$ and $P_{M2.9}$ equal to $P_{M2.1}$; $P_{M2.2}, P_{M2.3}, P_{M2.6}, P_{M2.7}, P_{M2.10}$ and $P_{M2.11}$ equal to $P_{M1.2}$.

B. Mathematical Model for the Magnetomotive sources.

The mathematical model proposed for the magnetomotive sources that represent the magnet of the generator, uses (4) and (5). The magnetomotive sources employed are non-ideal magnetomotive sources, so it is modeled by an ideal magnetomotive source in series with a reluctance for each part of the magnet. Fig. 7(a) presents these magnetomotive sources. There are 24 magnetomotive sources that mathematically represent half of the PMSG magnet: 12 to represent the top layer of the magnet and another 12 to represent the bottom layer of the magnet. The reluctances that seek to model the flux leakage from one magnet to another also can be seen, now in detail. By the analysis of Fig. 7(a), it is noted that there is a pattern for the representation of each region of the magnet. There are three types of magnetomotive sources: sources that are aligned with the tooth body, sources that are aligned with the tooth tips and sources that are aligned with the slot openings.
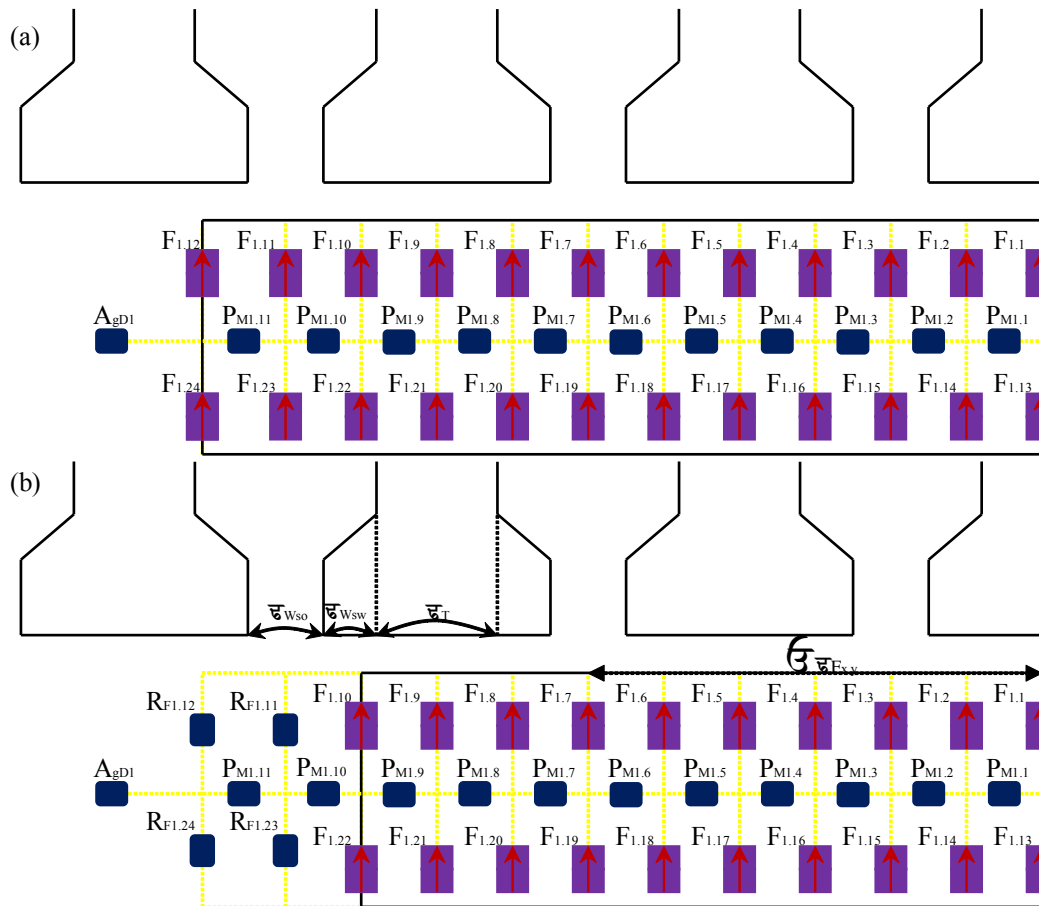
Fig. 7. Magnetomotive sources proposed for the modeling of the PM of the PMSG.

The magnetomotive sources: $F_{1.1}$, $F_{1.5}$, $F_{1.9}$, $F_{1.13}$, $F_{1.17}$ and $F_{1.21}$ are aligned with the tooth body and the expression for calculating the reluctance area of this source depends on the angle occupied by each tooth (θ_T). The magnetomotive sources: $F_{1.2}$, $F_{1.4}$, $F_{1.6}$, $F_{1.8}$, $F_{1.10}$, $F_{1.12}$, $F_{1.14}$, $F_{1.16}$, $F_{1.18}$, $F_{1.20}$, $F_{1.22}$ and $F_{1.24}$ are aligned with the tooth tips and the expression for calculating the reluctance area of these sources depends on the angle occupied by the tooth tip ($\theta_{W_{Sw}}$). Finally, the magnetomotive sources: $F_{1.3}$, $F_{1.7}$, $F_{1.11}$, $F_{1.15}$, $F_{1.19}$ and $F_{1.23}$ are aligned with the slot opening and the equation for calculating the reluctance area of these sources depends on the angle occupied by the slot opening ($\theta_{W_{So}}$). The equation for calculating the magnetomotive source (F_{mm}) and reluctance (R) that represent each of the 24 non-ideal magnetomotive sources ($F_{x.y}$) illustrated in Fig. 7(a), are shown in Table III.
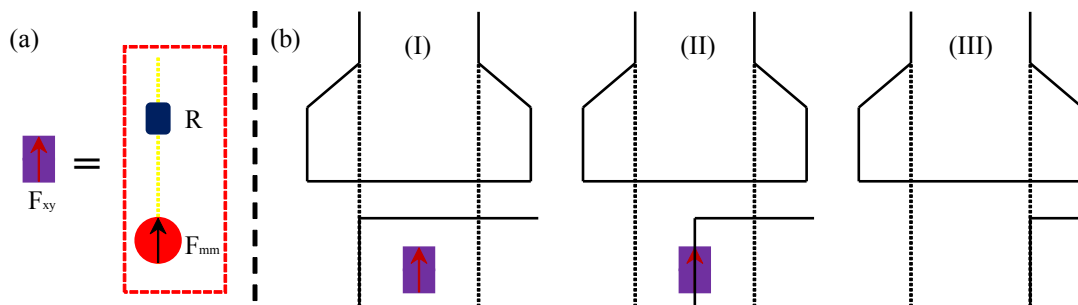

Fig. 8. Magnetomotive sources proposed for modeling the PM of the PMSG.

TABLE III. EQUATIONS USED TO CALCULATE THE LENGTH AND AREA OF THE AIR-GAP RELUCTANCES

Magnetomotive Source	Length (m)	Area (m²)
$F_{1.1}$ $F_{1.13}$	$\dfrac{h_{PM}}{2}$	$\left(\dfrac{W_{PM}}{2}\right) \bullet \left(\dfrac{\frac{\theta_T}{2}}{\frac{\alpha_{Pef}}{2}}\right) \bullet L_A$
$F_{1.5}$ $F_{1.9}$ $F_{1.17}$ $F_{1.21}$	$\dfrac{h_{PM}}{2}$	$\left(\dfrac{W_{PM}}{2}\right) \bullet \left(\dfrac{\frac{\theta_T}{2}}{\frac{\alpha_{Pef}}{2}}\right) \bullet L_A$
$F_{1.2}$ $F_{1.4}$ $F_{1.6}$ $F_{1.8}$ $F_{1.10}$ $F_{1.12}$ $F_{1.14}$ $F_{1.16}$ $F_{1.18}$ $F_{1.20}$ $F_{1.22}$ $F_{1.24}$	$\dfrac{h_{PM}}{2}$	$\left(\dfrac{W_{PM}}{2}\right) \bullet \left(\dfrac{\theta_{W_{Sw}}}{\frac{\alpha_{Pef}}{2}}\right) \bullet L_A$
$F_{1.3}$ $F_{1.7}$ $F_{1.11}$ $F_{1.15}$ $F_{1.19}$ $F_{1.23}$	$\dfrac{h_{PM}}{2}$	$\left(\dfrac{W_{PM}}{2}\right) \bullet \left(\dfrac{\theta_{W_{So}}}{\frac{\alpha_{Pef}}{2}}\right) \bullet L_A$

As the magnetomotive sources are presented in Fig. 7(a), the RN presents good results and maintains the accuracy in cases where the magnet height is modified. However, when the magnet width is changed, this formulation starts to lose its generalization characteristic. To solve this problem, it is valid to compare Fig. 7(a) with Fig. 7(b). It can be seen that in the second case, the magnet is narrower, therefore, the contribution of magnetic flux from magnetomotive sources $F_{1.11}$, $F_{1.12}$, $F_{1.23}$ e $F_{1.24}$ must be zero. Keeping in mind that non-ideal magnetomotive sources $F_{x.y}$ are being used, there are two ways to reduce the contributions of the sources when the magnet reduces its width: including a reluctance in parallel with each non-ideal magnetomotive source or reducing the flux value provided by the magnetomotive source (modifying the magnetic induction of the non-ideal source).

In the first case, with the inclusion of the air reluctance in parallel with the non-ideal source, the width that would be discounted from the magnetomotive source area is added to the area of this reluctance. Thus, the magnetic flux path is maintained, even when the width of the magnetomotive source is zero. However, this option requires the inclusion of an air reluctance in parallel with each magnetomotive source, resulting in a significant increase of elements. To avoid increasing the number of elements, a strategy is employed to reduce the magnetic flux produced by the ideal magnetomotive source, in proportion to the reduction of the PM width. With this, even if the magnetic flux supplied by the source is zero, the series reluctance of the source is maintained, as seen in Fig. 7(b). Therefore, a term in the calculation of the ideal magnetomotive sources F_{mm} was included, reducing the magnetic induction of the magnet proportionally to the reduction of the magnet width. This reduction of the magnetic flux is just a proposed mathematical model because physically, the operative induction of the magnet is constant.

In order to measure the reduction that each magnetomotive source must have in its flux, it is necessary to know how many teeth are in front of the magnet surface. To make the explanation clearer, Fig. 8(b) will be used. To enable the magnet to vary freely within a modeled region by a single

magnetomotive source, the RN must be able to calculate the flux produced by the magnetomotive source for three cases:

- when the magnetomotive source is completely inside the magnet (I);
- when the magnet ends up within the region modeled by that magnetomotive source (II);
- when the magnet does not reach the region modeled by that source (case III).

With (5), the RN is not able to calculate the change in magnetic flux effectively due to magnet with variation. Therefore, the expression for calculating the F_{mm} has to be modified. In addition to the variables already presented in (4), the term $\Delta_{\theta Fx.y}$ is included to take into account the possible changes in the width of the magnet, without excluding any path of magnetic flux present in the reluctance network.

$$F_{mm} = \frac{B_{op}}{\mu_0 \bullet \mu_r} \bullet l_r \bullet (1 - \Delta_{\theta Fx.y}) \tag{6}$$

$$\Delta_{\theta Fx.y} = \left(\sum \theta_{Fx.y} - \frac{\alpha_{Pef}}{2} \right) \bullet \frac{1}{\theta_{Fx.y}} \tag{7}$$

The calculation of the factor $\Delta_{\theta Fx.y}$ consists of a ratio between the angular distance from the magnet center to each magnetomotive source ($\sum \theta_{Fx.y}$) minus the effective pole pitch (α_{Pef}) divided by the angle that each magnetomotive source occupies ($\theta_{Fx.y}$). The angular distance between the center of the magnet and the magnetomotive source $F_{1.7}$ is indicated in Fig. 7(b). It is clear that this angular distance can be written as a sum of the angles occupied by the magnetomotive sources between the center of the tooth to the source $F_{1.7}$. For the source $F_{1.7}$, the value of $\sum \theta_{F1.7}$ is expressed as the sum of two times $\theta_{W_{so}}$, three times $\theta_{W_{Sw}}$ and one and a half times θ_T and the angle occupied by the source $\theta_{F1.7}$ is $\theta_{W_{so}}$. Now, it is possible to determine the value of $\Delta_{\theta F1.7}$ and define the contribution of the source $F_{1.7}$ given the effective pole pitch that the magnet assumes. Table IV summarizes the expressions of $\sum \theta_{Fx.y}$ and $\theta_{Fx.y}$ for each of the magnetomotive sources present in the RN.

TABLE IV. EXPRESSIONS OF $\sum \theta_{Fx.y}$ AND $\theta_{Fx.y}$ FOR EACH OF THE MAGNETOMOTIVE SOURCES.

Magnetomotive Source	$\sum \boldsymbol{\theta_{Fx.y}}$	$\boldsymbol{\theta_{Fx.y}}$
$F_{1.1}$ $F_{1.13}$ $F_{2.1}$ $F_{2.13}$	$0.5 \cdot \theta_T$	$0.5 \cdot \theta_T$
$F_{1.2}$ $F_{1.14}$ $F_{2.2}$ $F_{2.14}$	$\theta_{W_{Sw}} + 0.5 \cdot \theta_T$	$\theta_{W_{Sw}}$
$F_{1.3}$ $F_{1.15}$ $F_{2.3}$ $F_{2.15}$	$\theta_{W_{So}} + \theta_{W_{Sw}} + 0.5 \cdot \theta_T$	$\theta_{W_{So}}$
$F_{1.4}$ $F_{1.16}$ $F_{2.4}$ $F_{2.16}$	$\theta_{W_{So}} + 2 \cdot \theta_{W_{Sw}} + 0.5 \cdot \theta_T$	$\theta_{W_{Sw}}$
$F_{1.5}$ $F_{1.17}$ $F_{2.5}$ $F_{2.17}$	$\theta_{W_{So}} + 2 \cdot \theta_{W_{Sw}} + 1.5 \cdot \theta_T$	θ_T
$F_{1.6}$ $F_{1.18}$ $F_{2.6}$ $F_{2.18}$	$\theta_{W_{So}} + 3 \cdot \theta_{W_{Sw}} + 1.5 \cdot \theta_T$	$\theta_{W_{Sw}}$
$F_{1.7}$ $F_{1.19}$ $F_{2.7}$ $F_{2.19}$	$2 \cdot \theta_{L_{ra}} + 3 \cdot \theta_{W_{Sw}} + 1.5 \cdot \theta_T$	$\theta_{W_{So}}$
$F_{1.8}$ $F_{1.20}$ $F_{2.8}$ $F_{2.20}$	$2 \cdot \theta_{W_{So}} + 4 \cdot \theta_{W_{Sw}} + 1.5 \cdot \theta_T$	$\theta_{W_{Sw}}$
$F_{1.9}$ $F_{1.21}$ $F_{2.9}$ $F_{2.21}$	$2 \cdot \theta_{W_{So}} + 4 \cdot \theta_{W_{Sw}} + 2.5 \cdot \theta_T$	θ_T
$F_{1.10}$ $F_{1.22}$ $F_{2.10}$ $F_{2.22}$	$2 \cdot \theta_{W_{So}} + 5 \cdot \theta_{W_{Sw}} + 2.5 \cdot \theta_T$	$\theta_{W_{Sw}}$
$F_{1.11}$ $F_{1.23}$ $F_{2.11}$ $F_{2.23}$	$3 \cdot \theta_{W_{So}} + 5 \cdot \theta_{W_{Sw}} + 2.5 \cdot \theta_T$	$\theta_{W_{So}}$
$F_{1.12}$ $F_{1.24}$ $F_{2.12}$ $F_{2.24}$	$3 \cdot \theta_{W_{So}} + 6 \cdot \theta_{W_{Sw}} + 2.5 \cdot \theta_T$	$\theta_{W_{Sw}}$

The factor $\Delta_{\theta Fx.y}$ is determined with (7) so that its value is within the range of [0,1] if the magnetomotive source contains the edge of the PM. With this, it is possible to account for the flux value that must be taken from this source, due to the absence of a magnet in the entire width of the source, case II of Fig. 8(b). For the other sources, the magnet fills the entire domain of the magnetomotive source (the entire domain of the magnetomotive source is within the PM) or the magnet does not reach the domain represented by the magnetomotive source (the entire domain of the magnetomotive source is air), cases I and III, in Fig. 8(b). For case I, the values of $\Delta_{\theta Fx.y}$ start to assume values less than zero, while for case III the values start to be greater than 1. Both situations are undesired and do not represent the physical phenomenon correctly, therefore, a rule is defined for the calculation of $\Delta_{\theta Fx.y}$.

$$\Delta_{\theta Fx.y} = \begin{cases} 0, & \Delta_{\theta Fx.y} < 0 \\ \Delta_{\theta Fx.y}, & 0 < \Delta_{\theta Fx.y} < 1 \\ 1, & \Delta_{\theta Fx.y} > 1 \end{cases} \tag{8}$$

The calculation of the value of each non-ideal magnetomotive source $F_{x.y}$ still takes into account the relative permeability (μ_r) of the PM, considered equal to 1, since the magnet has a permeability very close to air. One of the inputs of the RN is the operative induction of the magnet, used in the calculation of the magnitude of the ideal magnetomotive sources. The magnetic flux density provided by the PM depends on the magnetic circuit in which it is inserted, thus, it depends on the constructive characteristics of the PMSG. In order to turn it parametric, a trend line is developed for the magnetic flux density as a function of the permeance coefficient, using a finite set of points. The operative induction of the magnetomotive sources can be calculated for any value that the permeance coefficient assumes, limited to the maximum values and minimums used to build the trend line.

To obtain this trend line, several operating points of the Neodymium-Iron-Boron magnet, grade N42, at a constant temperature of 80°C were gathered. The expression used for the calculation of the operative induction resulted in a 5th order polynomial presented below and the data used in the elaboration of the trend line are presented in Table V.

TABLE V. DATASET USED ON THE TREND LINE OF THE OPERATIVE INDUCTION AS A FUNCTION OF THE PERMEANCE COEFFICIENT

Permeance Coefficient	2	2.2	2.4	2.6	2.8	3	3.2	3.4	3.6	3.8
Operative Induction (T)	0.7920	0.8180	0.8410	0.8620	0.8800	0.8970	0.9120	0.9260	0.9390	0.9500
Permeance Coefficient	4	4.2	4.4	4.6	4.8	5	5.2	5.4	5.6	5.8
Operative Induction (T)	0.9610	0.9710	0.9800	0.9890	0.9960	1.0040	1.0110	1.0170	1.0240	1.0290
Permeance Coefficient	6	6.2	6.4	6.6	6.8	7	7.2	7.4	7.6	7.8
Operative Induction (T)	1.0350	1.0400	1.0450	1.0490	1.0540	1.0580	1.0620	1.0660	1.0690	1.0730
Permeance Coefficient	8	8.2	8.4	8.6	8.8	9	9.2	9.4	9.6	9.8
Operative Induction (T)	1.0760	1.0790	1.0820	1.0850	1.0880	1.0900	1.0930	1.0950	1.0980	1.1000
Permeance Coefficient	10	10.5	11	11.5	12	-	-	-	-	-
Operative Induction (T)	1.1020	1.1080	1.1120	1.1170	1.1531	-	-	-	-	-

This expression used for the calculation of the operative induction is function of the permeance coefficient P_c, calculated using (1).

$$B_{op} = 0.0000244 \cdot P_c{}^5 - 0.000881 \cdot P_c{}^4 + 0.01267 \cdot P_c{}^3 - 0.0935 \cdot P_c{}^2 + 0.3852 \cdot P_c + 0.3075 \tag{9}$$

IV. RESULTS AND DISCUSSIONS

The generated reluctance network was implemented in one of the internal modules of the CADES software, namely RELUCTOOL [20]. The software inputs are the dimensions presented in Fig. 1 used to calculate the lengths and areas of each reluctance. The software solves the non-linear system (3) by Newton's method and provides the magnetic flux in all elements of the RN. To evaluate the quality of the results obtained by the reluctance network, numerical simulations with FEM (performed with EFCAD) were performed and a comparison between these two methods was performed. Four PMSG's with different dimensions are simulated in order to verify the generalization capacity of the RN. Three generators have 36 slots and 6 poles and the last one has 48 slots and 8 poles. Table VI presents the main dimensions of all the generators (presented in the Fig. 1).

TABLE VI. MAIN DIMENSIONS OF THE FOUR SIMULATED GENERATORS

Dimension	PMSG 1 (mm)	PMSG 2 (mm)	PMSG 3 (mm)	PMSG 4 (mm)
D_{re}	287.3	287.3	289.0	287.3
D_{ri}	163.9	163.9	165.6	188.4
L_{AG}	4.3	4.3	3.4	4.3
h_{Sy}	66.2	66.2	66.2	49.7
h_{PM}	12.7	12.7	12.7	12.7
h_S	36.6	36.6	36.6	27.5
h_{Sw}	2.8	2.8	2.8	2.1
h_{So}	2.8	2.8	2.8	2.1
W_{So}	4.2	4.2	4.2	3.0
W_{Sw}	4.8	4.8	4.8	3.6
α_p	60.0°	60.0°	60.0°	45.0°
α_{Pef}	54.0°	45.0°	54.0°	40.5°
α_S	10.0°	10.0°	10.0°	7.5°
θ_{St}	5.2°	5.2°	5.2°	3.9°

The proposed changes for PMSG 2, PMSG 3 and PMSG 4 were made in relation to PMSG 1:

- PMSG 2: reduction of the effective pole pitch, but keeping the other dimensions of PMSG 1;
- PMSG 3: reduction in the length of the machine air gap, and keeping the stator dimensions of PMSG 1;
- PMSG 4: increase in the number of slots and poles, with some differences compared to PMSG 1.

The comparison between the magnetic flux values calculated by the RN and calculated by the FEM were made at nine regions, highlighted by red dotted ellipses in Fig. 5 and Fig. 6. The regions chosen to carry out the validation are: the rotor yoke (ϕ_{R_y}), the center of permanent magnet 1 ($\phi_{P_{M1}}$), the air gap below teeth 1, 2 and 3 ($\phi_{A_{g1}}$, $\phi_{A_{g2}}$ e $\phi_{A_{g3}}$), the center of teeth 1, 2 and 3 ($\phi_{T_{b1}}$, $\phi_{T_{b2}}$ e $\phi_{T_{b3}}$) and the stator yoke (ϕ_{S_y}). Table VII and Table VIII show the comparison of the magnetic flux values for the 9 regions proposed in Fig. 5 and Fig. 6 of all four generators with dimensions presented in Table VI.

TABLE VII. MAGNETIC FLUX VALUES OBTAINED WITH RELUCTANCE NETWORK AND THE FINITE ELEMENTS SIMULATIONS OF PMSG 1 AND PMSG 2

Generator	PMSG 1 (mWb)			PMSG 2 (mWb)		
Region	RN	FEM	Difference	RN	FEM	Difference
$\phi_{T_{b1}}$	2.06	2.04	0.96%	2.06	2.04	0.97%
$\phi_{T_{b2}}$	4.11	4.08	0.82%	4.08	4.05	0.87%
$\phi_{T_{b3}}$	4.01	3.94	1.88%	3.08	3.07	0.53%
ϕ_{S_y}	10.19	10.02	1.67%	9.23	9.12	1.15%
ϕ_{R_y}	11.15	11.29	-1.21%	9.29	9.34	-0.49%
$\phi_{A_{g1}}$	1.85	1.79	3.53%	1.85	1.79	3.44%
$\phi_{A_{g2}}$	3.70	3.58	3.42%	3.70	3.58	3.35%
$\phi_{A_{g3}}$	3.63	3.50	3.76%	2.83	2.75	2.95%
$\phi_{P_{M1}}$	11.15	11.30	-1.37%	9.23	9.12	1.15%

TABLE VIII. MAGNETIC FLUX VALUES OBTAINED WITH RELUCTANCE NETWORK AND THE FINITE ELEMENTS SIMULATIONS OF PMSG 3 AND PMSG 4

Generator	PMSG 3 (mWb)			PMSG 4 (mWb)		
Region	RN	FEM	Difference	RN	FEM	Difference
$\phi_{T_{b1}}$	2.20	2.14	2.68%	1.55	1.54	0.54%
$\phi_{T_{b2}}$	4.37	4.27	2.47%	3.08	3.06	0.53%
$\phi_{T_{b3}}$	4.28	4.14	3.34%	2.97	2.90	2.25%
ϕ_{S_y}	10.85	10.51	3.18%	7.59	7.48	1.53%
ϕ_{R_y}	11.87	11.81	0.53%	8.36	8.59	-2.62%
$\phi_{A_{g1}}$	1.98	1.88	5.02%	1.39	1.35	2.91%
$\phi_{A_{g2}}$	3.95	3.76	4.90%	2.78	2.70	2.74%
$\phi_{A_{g3}}$	3.89	3.71	4.70%	2.69	2.59	4.14%
$\phi_{P_{M1}}$	11.87	11.82	0.40%	8.36	8.57	-2.47%

Analyzing the results shown in Table VII and Table VIII, it is verified that the magnetic flux values computed by the RN are close to those obtained with the FEM, since the deviations do not exceed 5.02%, the variation range for the deviation values are between 0.4 to 5.02%. It appears that the highest deviation values for the 4 generators are observed in the air gap region. PMSG 1, the generator used as reference for the generation of the RN, has the largest deviations for the air gap region, with the largest difference being found for the air gap of tooth 3. For PMSG 2, there is a reduction in the value of the magnetic flux in the air gap of the tooth 3 and in the center of the tooth 3. This is due to the reduction of the magnet width, since some magnetomotive sources below the tooth three are no longer active (shown in Fig. 5). This result validates the proposed calculation methodology for the magnetomotive sources, since the magnet width was changed, and the maximum deviation values remained close to 3.5%.

For PMSG 3, there is an increase in the magnetic flux values in both the air gap and iron regions, when compared to PMSG 1. This occurs because the PC of the generator was increased (the height of the PM was maintained while the length of the air gap was reduced) and the other dimensions were kept, hence the flux values increased and the PMSG 3 operates more saturated than the PMSG 1. Even in this condition, the reluctance network kept the deviation values in an acceptable range, when compared to FEM. For the air gap region, the largest deviation observed was 5.02% in the air gap of tooth 1, while in the iron region, the largest deviation seen was 3.34% for the center of tooth 3.

For PMSG 4, with the increase in the number of poles and stator slots, significant changes are noticed when comparing the dimensions with the of PMSG 1 ones. Even with all changes, the deviations for the magnetic flux values remained below 5% for all calculated regions. The largest deviations occur in the air gap region, being between 2.74% and 4.14% and the smallest deviations are seen for the region of the center of the teeth, ranging from 0.53% to 2.25%. The proposed changes for PMSG 4 allow us to conclude that the proposed RN can be used for machines with different number of poles, as long as the proportion of the number of teeth per pole (6) is maintained.

As a final validation of the performance of the reluctance network, the induced internal voltage (E_a) of the PMSG 1 was calculated, using the reluctance network and the finite element simulation. For the calculation of E_a, the following characteristics are considered for the PMSG 1: distributed diamond windings, double layer, with a shortening of the armature coil pitch of 2/3, 6 turns per coil and 2 coils per pole and per phase. The module of the linked flux obtained with the reluctance network uses the following formula:

$$|\phi_L| = 2 \cdot \phi_{T_{b1}} + 2 \cdot \phi_{T_{b2}} + \phi_{T_{b3}} \tag{10}$$

As there are 2 coils per pole and per phase, it is necessary to calculate the total flux linking adding the flux of the first coil with a spatial delay equal to 0° and the second coil considering a lag with a spatial delay of 10°. Thus, the expression for the total linked flux is:

$$\phi_{L_T} = |\phi_L| + |\phi_L| \cdot e^{i \cdot \frac{\pi}{18}} \tag{11}$$

The RMS value of the induced internal voltages and the computational cost for each method (RN and FEM) are presented in Table IX. The deviation for the induced internal voltage is even smaller than the deviations of magnetic flux, seen in Table VII. In addition, the reluctance network has presented a computational cost 20 times lower than the FEM one. It is worth mentioning that in an optimization, a process in which the machine needs to be simulated for several positions and for a number of iterations of the optimization algorithm, a reduction in computational cost as seen in this comparison can represent a significant reduction in the total simulation time. Furthermore, once the RN is achieved, it can be used for similar machines (same topology and number of slots per pole) without any additional work.

TABLE IX. RMS VALUE OF THE INDUCED INTERNAL VOLTAGES AND COMPUTATIONAL COST FOR EACH METHOD

Induced Internal Voltage (V)			Computational Time (s)		
RN	FEM	Difference	RN	FEM	Ratio
312.576	312.12	0.14%	0.09	1.80	20

It is worth mentioning that in an optimization, the process in which the machine needs to be simulated for several positions and for all iterations of the optimization algorithm, a reduction in computational cost as seen in this comparison can represent a significant reduction in simulation time. Finally, a comparison is made between the E_a curve obtained with FEM and the E_a curve obtained with RN, considering a perfect sinusoidal waveform (without harmonic content) in which the peak value was obtained with the RN earlier. The FEM and the RN E_a curve correspond respectively to the solid line and dashed line in Fig. 9. The similarity in the behavior of the curves is observed because the total harmonic distortion of the E_a of the PMSG 1 is not greater than 4%. If the harmonic content was greater, the curves would be different and the deviation in the calculation of E_a would be greater.
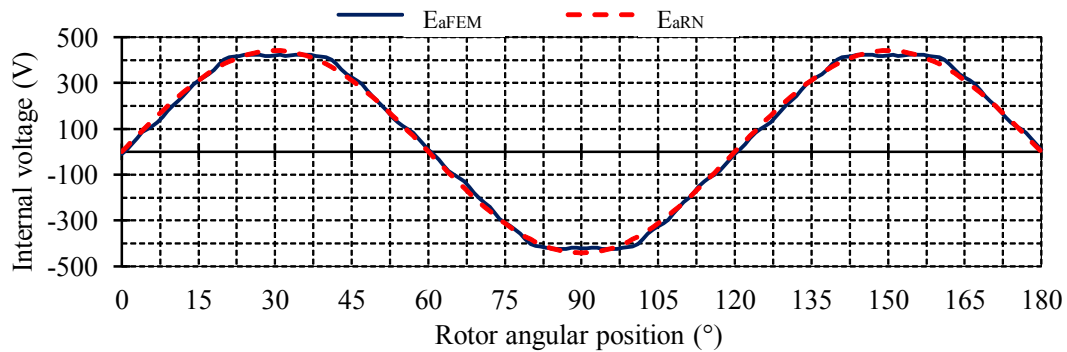

Fig. 9. Comparison between FEM and RN Ea waveforms.

V. CONCLUSIONS

This paper presents a methodology for the generation of static RN with magnetomotive sources only in the rotor. The generated reluctance network using the proposed methodology is capable of calculating the magnetic flux of a surface mounted permanent magnet synchronous generator operating at no load, in different regions of the generator. With the obtained fluxes, the value of the flux linked by the stator coils was calculated and the induced internal voltage of the machine was obtained. In both situations, the values of the deviations presented by the reluctance network, when compared with the finite element method, were satisfactory. Furthermore, this network can be applied to calculate the magnetic flux density at various points and the value of the generator no-load losses. Thus, the proposed network is a very useful tool in the design and analysis stage of a surface mounted permanent magnet synchronous generator.

The proposed methodology has been validated by changing the reference generator (PMSG1) dimensions (in PMSG 2, PMSG 3 and PMSG 4) and its overall saturation (in PMSG4) and the robustness of the reluctance network have been proven. The proposed network can be coupled to an

optimization algorithm, given its generalization capacity and the reduction of the computational cost provided makes possible the development of an optimal design tool of a PMSG. The development process of the reluctance network is onerous. However, once is completed, it can be used in other similar machines to significantly reduce the computational time of optimized projects.

REFERENCES

[1] J. Hendershot e T. J. Miller, Desing of Brushless Permanent-Magnet Machines, 2ª ed., M. D. Book, Ed., Venice: Motor Desing Book, 2010.

[2] I. Boldea, Synchronous Generator, II ed., T. F. Group, Ed., Timisoara: CRC Press, 2016.

[3] V. Ostovic, "Computation of Saturated Permanent-Magnet AC Motor Performance by Means of Magnetic Circuits," *IEEE Transactions on Industry Applications,* vol. 23, no. 5, pp. 836-841, 1987.

[4] T. Bazzo, J. Kolzer, R. Carlson, F. Wurtz, L. Gerbaud, "Multiphysics Design Optimization of a Permanent Magnet Synchronous Generator," *IEEE Transactions on Industrial Electronics,* vol. 64, no. 12, pp. 9815-9823, 2017.

[5] V. Moura, P. C. d. N. Júnior, G. G. Menezes, T. d. P. M. Bazzo, "Procedimento para criar redes de relutâncias para modelar as reatâncias de eixo direto e em quadratura de geradores síncronos," em *XIV Congresso Brasileiro de Eletromagnetismo (MOMAG)*, Rio de Janeiro, 2020.

[6] J.-Y. Song, J. H. Lee, D.-W. Kim, Y.-J. Kim, S.-Y. Jung, "Analysis and Modeling of Permanent Magnet Variable Flux Memory Motors Using Magnetic Equivalent Circuit Method," *IEEE Transactions on Magnetics,* vol. 53, no. 11, pp. 1-5, 2017.

[7] K. Nakamura, S. Hisada, K. Arimatsu, T. Ohinata, K. Sakamoto, O. Ichinokura, "Iron Loss Calculation in a Three-Phase-Laminated-Core Variable Inductor Based on Reluctance Network Analysis," *IEEE Transactions on Magnetics,* vol. 45, no. 10, pp. 4781 - 4784, 2009.

[8] Y. Yoshida, K. Nakamura, O. Ichinokura, "A Method for Calculating Eddy Current Loss Distribution Based on Reluctance Network Analysis," *IEEE Transactions on Magnetics,* vol. 47, no. 10, pp. 4155-4158, 2011.

[9] L. Zhu, S. Jiang, Z. Q. Zhu e C. C. Chan, "Analytical Modeling of Open-Circuit Air-Gap Field Distributions in Multisegment and Multilayer Interior Permanent-Magnet Machines," *IEEE Transactions on Magnetics,* vol. 45, no. 8, pp. 3121-3130, 2009.

[10] C. Ma, J. Zhang, J. Wang, N. Yang, Q. Liu, S. Zuo, "Analytical Model of Open-Circuit Air-Gap Field Distribution in Interior Permanent Magnet Machines Based on Magnetic Equivalent Circuit Method and Boundary Conditions of Macroscopic Equations," *IEEE Transactions on Magnetics,* vol. 57, no 3, pp. 1-9, 2021.

[11] O. Taqavi e N. Taghavi, "Development of a Mixed Solution of Maxwell's Equations and Magnetic Equivalent Circuit for Double-Sided Axial-Flux Permanent Magnet Machines," *IEEE Transactions on Magnetics,* vol. 57, no 4, pp. 1-11, 2021.

[12] G. Wang, P. Wang, X. Wang, "Equivalent Magnetic Circuit Reluctance Optimization for Rotor Loss Reduction in Permanent Magnet Synchronous Motor for UPS-FESS," *IEEE Access,* vol. 8, pp. 107593-107600, 2020.

[13] H. Dogan, L. Garbuio, H. Nguyen-Xuan, B. Delinchant, A. Foggia, F. Wurtz, "Multistatic Reluctance Network Modeling for the Design of Permanent-Magnet Synchronous Machines," *IEEE Transactions on Magnetics,* vol. 49, no. 5, pp. 2347-2350, 2013.

[14] H. Xie, G. Krebs, M. H. Hassan, M. Zhang, C. Marchand, Z. Ren, "A New Reluctance Network-Based Method With Complementary Distributed Magnetomotive Forces," *IEEE Transactions on Magnetics,* vol. 55, no. 6, pp. 1-5, 2019.

[15] D. Cao, W. Zhao, J. Ji, L. Ding, J. Zheng, "A Generalized Equivalent Magnetic Network Modeling Method for Vehicular Dual-Permanent-Magnet Vernier Machines," *IEEE Transactions on Energy Conversion,* vol. 34, no. 4, pp. 1950-1962, 2019.

[16] S. Wu, T. Shi, L. Guo, H. Wang, C. Xia, "Accurate Analytical Method for Magnetic Field Calculation of Interior PM Motors," *IEEE Transactions on Energy Conversion,* vol. 36, no. 1, pp. 325-337, 2021.

[17] Z. Li, X. Huang, L. Wu, H. Zhang, T. Shi, Y. Yan, B. Shi e G. Yang, "An Improved Hybrid Field Model for Calculating On-Load Performance of Interior Permanent-Magnet Motors," *IEEE Transactions on Industrial Electronics,* vol. 68, no. 10, pp. 9207-9217, 2021.

[18] M. Bash, J. Williams, S. Pekarek, "Incorporating Motion in Mesh-Based Magnetic Equivalent Circuits," *IEEE Transactions on Energy Conversion,* vol. 25, no. 2, pp. 329 - 338, 2010.

[19] J. P. A. Bastos, N. Sadowski, EFCAD - Electromagnetic Fields Computer Aided Design, 1ª ed., UFSC, Ed., Florianópolis: UFSC, 2008.

[20] B. d. Peloux, L. Gerbaud, F. Wurtz, V. Leconte, F. Dorschner, "Automatic Generation of Sizing Static Models Based on Reluctance Networks for the Optimization of Electromagnetic Devices," *IEEE Transactions on Magnetics,* vol. 42, no. 4, pp. 715-718, 2006.